Energy 239 (2022) 122145

Contents lists available at ScienceDirect

Energy

journal homepage: www.elsevier.com/locate/energy

Investigation of the mechanical damage of low rank coals under the impacts of cyclical liquid CO_2 for coalbed methane recovery

Jizhao Xu [a, b, c, **], Cheng Zhai [a, b, c, *], Pathegama Gamage Ranjith [d], Shuxun Sang [a], Yong Sun [b, c], Yuzhou Cong [b, c], Wei Tang [b, c], Yangfeng Zheng [b, c]

[a] Jiangsu Key Laboratory of Coal-based Greenhouse Gas Control and Utilization, China University of Mining and Technology, 221008, Xuzhou, Jiangsu, China
[b] Key Laboratory of Coal Methane and Fire Control, Ministry of Education, China University of Mining and Technology, 221116, Xuzhou, Jiangsu, China
[c] School of Safety Engineering, China University of Mining and Technology, 221116, Xuzhou, China
[d] Department of Civil Engineering, Building 60, Monash University, Clayton VIC 3800, Australia

ARTICLE INFO

Article history:
Received 14 April 2021
Received in revised form
24 August 2021
Accepted 21 September 2021
Available online 28 September 2021

Keywords:
Cracks
Liquid CO_2
Temperature shock
Gas adsorption
Damage accumulation

ABSTRACT

Liquid CO_2 enhanced coalbed methane recovery has been proposed for decades, and the accompanying effects of phase-transition and adsorption of liquid CO_2 slightly influenced the coal structure strength. Studying the coal strength variation under the effects of liquid CO_2 is of great significance for evaluating the selected liquid CO_2 injection parameters, CO_2 injectability, and coal cracking initiation capacity. However, the coupling effects of the temperature gradient and adsorption of cyclical liquid CO_2 on the coal strength have not been systematically studied. In this study, based on the cyclical liquid CO_2 fracturing experimental system, the low-rank coals were processed under the effects of liquid CO_2 with different cyclical parameters. Subsequently, a uniaxial compression test was carried out to investigate the mechanical responses of the processed coals under the sole and coupled effect of liquid CO_2 temperature and adsorption, respectively, using acoustic emission and strain gauge. The results showed that coals exhibited different destruction behaviours and fracture morphologies; for example, coals influenced by the sole effect showed an "axial separation" failure pattern, while liquid CO_2 coupling affected coals showed a "separation and spallation" destruction form. Compared to raw coals, the affected coals contained a larger ring count and accumulated energy J, indicating that thermal cycling induced by uneven temperature distribution enhanced the generation of new cracks and expansion of the original cracks, and the enlarged crack volume provided sufficient adsorption sites for CO_2 molecules to decrease the Gibbs free energy. The negative relationship between σ_c and cyclical parameters showed that the alternative temperature shock significantly degraded the cohesive strength among the grains with amounts of the damage accumulation, leading to tensile failure. The J_e/J_t and J_r/J_t scatters positively and negatively correlated with the corresponding cyclical (cycles and time) and mechanical parameters (E and σ_c), respectively, indicating that the more liquid CO_2 affected, the greater the damage accumulation, and the larger the destructive plastic region and lower the strain energy storage capacity, because of the synergy of the cold shock and gas adsorption. The research results provided theoretical guidance for optimizing liquid CO_2 injection parameters for balancing the investment and output benefit of coalbed methane.

1. Introduction

As an accompanying product of the coal forming process, coalbed methane (CBM) had always been regarded as a potential green environmental resource to ease the global energy shortage crisis [1,2]. During the gas extraction process, comparing the primary reservoir and critical desorption pressures determined the production system establishment, the coupling effect of effective stress

* Corresponding author. Jiangsu Key Laboratory of Coal-based Greenhouse Gas Control and Utilization, China University of Mining and Technology, 221008, Xuzhou, Jiangsu, China.
** Corresponding author. Jiangsu Key Laboratory of Coal-based Greenhouse Gas Control and Utilization, China University of Mining and Technology, 221008, Xuzhou, Jiangsu, China.
E-mail addresses: jizhao_xu@cumt.edu.cn (J. Xu), greatzc@cumt.edu.cn (C. Zhai).

https://doi.org/10.1016/j.energy.2021.122145
0360-5442/

and matrix shrinkage might make permeability to be in dynamic equilibrium as well as create the potential material and energy balance. Reservoir porosity-permeability determined gas migration; the larger the permeability, the smaller the flow resistance, and the larger the extraction efficiency [3–5]. However, this was not always the case. Significantly low permeability in the coal reservoir of China had been generally observed [6,7], thus, some permeability enhancement methods should be considered to improve the extraction capacity.

For decades, hydraulic or anhydrous fracturing technologies had been proposed and commercially applied for extraction enhancement, based on different fracturing mediums and various physical-chemical modification forms of the reservoirs [8–11]. Anhydrous fracturing methods mostly adopted gases [12,13], explosives [14], and thermal waves [15,16], etc., thus, providing their feasibility and effectiveness for improving the permeability. In China, abundant CBM reservoirs were distributed in the Northwest and Central China, where water resource shortage hindered the wide application of hydraulic fracturing. As an alternative to pressurised water, CO_2 was selected because of its better affinity to coal than CH_4, lower viscosity than fracturing fluids, and larger expansion volume than water [17,18]. In field applications, the intrinsic properties of different-phase CO_2 changed transiently at different formation depths (seen in Fig. 1), which was controlled by the combination of pressure and temperature [19]. Meanwhile, the cost input of CO_2 and output benefit of CH_4 should be considered to achieve the maximum production ratio by selecting a specific phase of CO_2.

Considering the economic input and engineering applications, liquid CO_2 was commonly injected into the reservoirs to enhance CBM recovery, and Silva et al. [20] considered this method to be an active and efficient injection model. Compared to gaseous and supercritical CO_2, liquid CO_2 had a greater liquid-gas expansion rate and did not require additional heating treatment, which could reduce the technical cost input [19,21]. When a large amount of cryogenic liquid CO_2 was injected into the reservoir, a potential heat transfer occurred at the interaction interface, with the phase transition of CO_2 taking place, and the larger density difference between the liquid and gas phases might cause the pressure-temperature reconstruction along the flow path [22]. The field trial test results reported that when liquid CO_2 (−53 °C) were injected into the Snøhvit and Sleipner wells (at a depth of 700 m) with an injection velocity of 400 kg/s, the temperature of the well bottom changed to −38 °C and −46 °C, respectively [23]. Ma et al. [24] proposed that the transient low-temperature effect of cyclical liquid CO_2 could alter the temperature field, and the accompanying volume shrinkage induced some tensile damage to destroy the coal structure by producing complex crack networks. Roy et al. [25] simplified the cyclical liquid CO_2 injection process by adopting an alternative CO_2 injecting (−50 °C, freezing) and temperature increasing (80 °C, heating) process, and pointed out that the thermal cycling of liquid CO_2 could create radial cracks. Teodorio [26] and Kaldal [27] agreed that thermal stress induced by temperature difference between the well surface and the surrounding rock could destroy the well stability, and the larger the temperature change, the greater the thermal stress. Li [28] found that the cooling radius positively correlated with the injection time by simulating the temperature distribution change during the liquid CO_2 injection process.

When liquid CO_2 were cyclically injected into the reservoirs, the periodic 'cold shock-thermal heat' process caused the matrix 'freeze-thaw'. This freezing-thawing process degraded the structural mechanics of the coal-rocks. Park et al. [29] revealed that the heat conductivity coefficient increased, and thermal expansion coefficient decreased with decreasing temperature. Zhang et al. [30] quantitatively expressed the coupling effect of freeze-thaw and loading on the total damage of red sandstone based on D-P failure criterion, and built a damage constitutive model for freeze-thaw rocks with residual strength. Yang et al. [31] found that coal

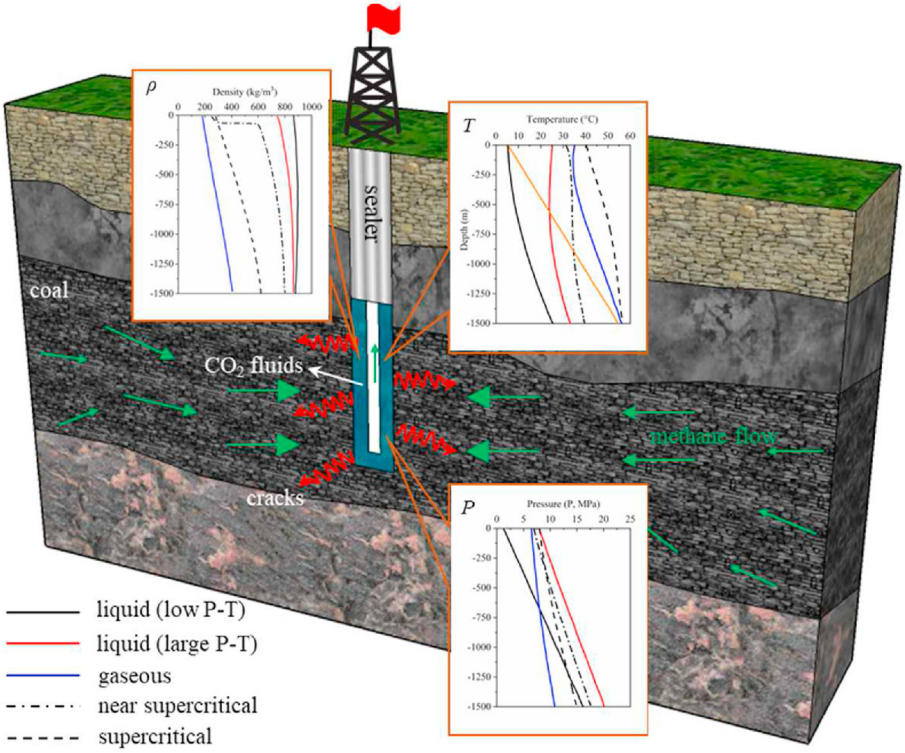

Fig. 1. CO_2 property changes at different depth in the field application (modified from Ref. [19]).

permeability was negatively correlated with low temperature, and positively correlated with water content. Qin et al. [32] reported that when coals were processed with cyclic liquid nitrogen, their compressive strength and elastic modulus decreased, while the porosity, Poisson's ratio, and damage variable increased. Xu et al. [33–35] used low-field nuclear magnetic resonance and infrared thermal imagery to test pore evolution and surface temperature, and found positive correlations between pore-permeability and cyclical parameters. Wen et al. [36,37] pointed out that the free water inside the coal matrix might freeze with volume expansion under the cryogenic effect of liquid CO_2, which extruded the original pore-crack structure and promoted the propagation and extension of the cracks.

Meanwhile, the phase transition of liquid CO_2 had been reported to make high-pressure CO_2 adsorption feasible, and the effect of its degradation on the coal strength had been demonstrated. Viete and Ranjith [38,39] studied the mechanical response behaviors of CO_2 adsorbed lignite under uniaxial or axial compressive conditions, and found that compressive stress and elastic modulus decreased under uniaxial conditions, and the degradation mechanism was quantitatively characterised based on Gibbs and Griffith theory [40]. Larsen [41] considered that the adsorbed CO_2 could be regarded as a plasticiser to facilitate coal structure reconstruction. Bai et al. [42] presented the formulas for calculating the critical expansion stress and weakening fracture of coals after CO_2 adsorption, based on solid surface energy and Griffith fracture theories.

In fact, liquid CO_2 enhanced CBM recovery process contained multiple mutually influenced physical fields. However, the coupling effect of thermal cycling and CO_2 adsorption on coal strength had been scarcely studied, which might create the blind selection of liquid CO_2 injection parameters. In this study, low-rank coals were treated with liquid CO_2 at different cycles and time, and the mechanical responses of the treated coals were subsequently investigated using uniaxial compression test. By comparing the failure pattern, the stress-strain curves, acoustic emission events, and energy evolution of different coals, the coupling degradation mechanism of liquid CO_2 and mechanical damages of the coals were systematically studied. The results provided guidelines to promote the wide application of liquid CO_2 enhanced CBM recovery.

2. Experimental system and procedure

2.1. Experimental specimen

The targeted coal specimens were obtained from the Shengli Coal Mine, Inner Mongolia, China. During the coal specimen preparation process, two aspects of screening were performed: first, the coal samples were drilled from the same block of the non-activated region within the reservoir to maintain good consistency by avoiding the apparent cleats or cracks [43]; second, the drilled specimens were tested using an ultrasonic velocimeter to remove the specimens with large differences by testing thrice at one site along different directions [44]. According to the Test Code for Physical and Mechanical Properties of Rocks (DZ/T 0276.18–2015) [45], the tested coals had a diameter and height of 50 and 100 mm, respectively, and the non-parallel and non-evenness errors of the upper and lower sides were less than 0.005 and 0.002 mm respectively. The moisture M_{ad}, ash A_{ad}, volatile V_{daf}, and fixed carbon contents FC_{ad} were 11.37%, 14.63%, 53.41%, and 20.59%, respectively. The vitrinite, inertinite, exinite, and mineral contents were 79.5%, 15.5%, 3.6%, and 1.4%, respectively, and vitrinite reflectance was 0.32, with the wave velocity of 1.53 km/s.

Fig. 2 showed the SEM and XRD images of lignite, using a scanning electron microscope (Quanta 250, USA FEI) and an X ray diffractometer (D8 ADVANCE, Germany Brock AXS Co., LTD), respectively. Some primary micro-cracks were distributed inside the matrix with different apertures and directions, and different crack widths along the same crack and different angles of the crack direction indicated that the cracks were not flat. The micro-cracks provided some flow paths for liquid CO_2 migration, also causing the accompanying flooding and displacement between CO_2 and CH_4. The XRD data displayed the relationship between diffracted intensity and two-theta, and $(Mg_{0.03}Ca_{0.97})CO_3$, $CaCO_3$, and $(Mg_{0.06}Ca_{0.94})CO_3$ existed (the reciprocal of the matching rate FOM less than 10), based on the standard card index, and its high matched-degree indicated the existence of some minerals, which was consistent with the observations of the SEM image. The minerals occupied in the cracks narrowed the crack width, and increased the roughness and tortuosity, where some thermal stress concentration easily occurred because of diverse thermal deformation capacities and anisotropy.

2.2. Experimental system

As described in a previous study [46], a cyclical liquid CO_2 fracturing simulation system could provide a contact reaction place for liquid CO_2 and coals under high pressure and low temperature conditions. By designing the different combinations of injection parameters, the coals were treated with the thermal cycling effect of cyclical liquid CO_2 to simulate the temperature shock process. The uniaxial compression test system (shown in Fig. 3) mainly consisted of a gravity deadweight loading system, an acoustic emission system, and a static strain gauge system. Based on the reliable servo control hydraulic system, the loading system had a rated load of not less than 600 kN, with a displacement resolution of lower than 0.2 μm and data collection frequency of higher than 1000 Hz. The acoustic emission system (PCIE-Q87-i2), produced by American Physical Acoustics Corporation, the United States, had a 32-channel host, and the S- and P-wave sensors had a frequency range of 300–480 and 125–750 kHz, respectively. The static strain gauge system (DH3821) had a bridge voltage accuracy of less than 0.1%, strain resolution of 1 με, and zero drift of less than 3 με/4 h. The analog-digital converter adopted a 24-bit Σ-ΔA/D converter.

2.3. Experimental procedure

Considering the limitations of the equipment function, the coupling that affected the process of liquid CO_2 was simulated in two steps: cyclical variable temperature treatment and CO_2 adsorption at normal temperature and high pressure. The raw coal core was labelled as LNA, and the CO_2 adsorbed raw-coal was labelled as $LNCO_2$, with an adsorption time of 48 h. The cores labelled as Lc-X/Lct-Y or Lca-X/Lcat-Y represented the cores treated under the cyclic temperature effect and temperature-adsorption coupling effect of CO_2, respectively, where X (5, 10, 15, 20, and 25) represented the cycle number, while Y (1, 2, 3, 4, and 5) represented the processing time. The cores labelled as Lca-X or Lcat-Y were also adsorbed with CO_2 for 48 h. The experimental design scheme was presented in Table 1.

As shown in Table 1, except the cores LNA and LNCO, the other cores were wrapped by films and placed into the autoclaves to react with liquid CO_2, and the cores (Lca and Lcat series) were subsequently nakedly immersed in CO_2 for full adsorption for 48 h. It was noticed that the cycle time included the freezing and heating times (both accounting for half), with a 'cold shock-heating' process being a cycle.

When the loading calibration ended, the displacement loading mode was selected, and the data acquisition frequency was set as

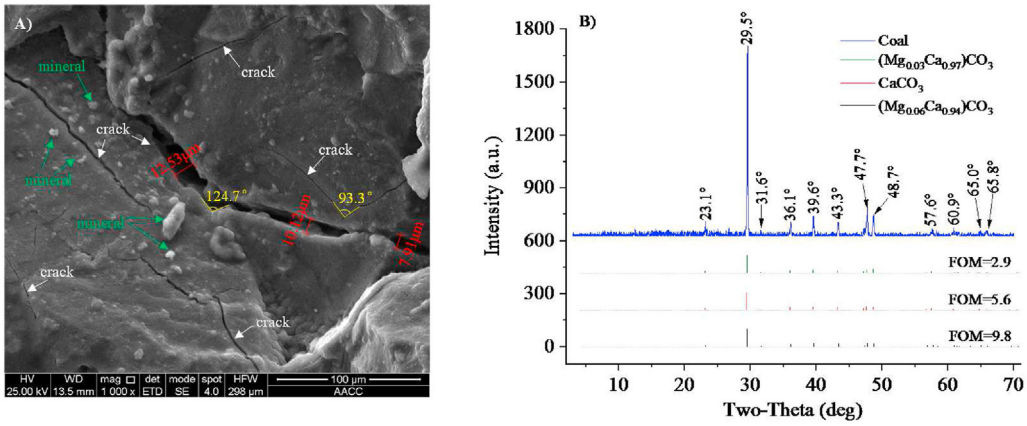

Fig. 2. Images of SEM and XRD for the coal.

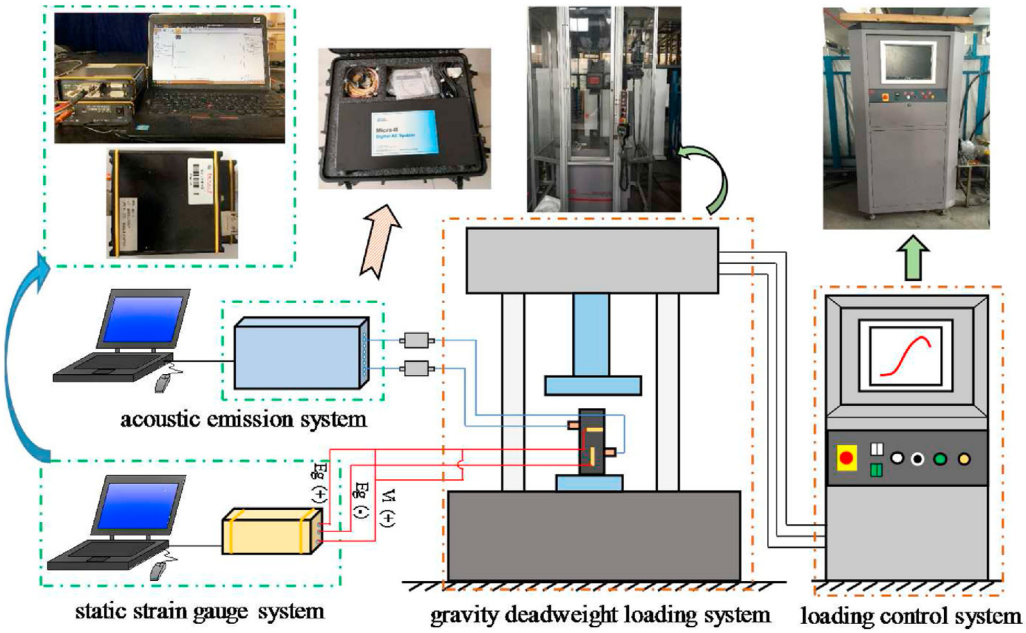

Fig. 3. Image of uniaxial compression test system.

Table 1
Experimental design of the coal mechanical test.

	cycle number	cycle time	CO_2 adsorption		cycle number	cycle time	CO_2 adsorption
LNA	–	–	–		–	–	–
$LNCO_2$	–	–	48 h		–	–	–
Lc-5	5	2 h	–	Lct-1	15	1 h	–
Lc-10	10		–	Lct-2		2 h	–
Lc-15	15		–	Lct-3		3 h	–
Lc-20	20		–	Lct-4		4 h	–
Lc-25	25		–	Lct-5		5 h	–
Lca-5	5	2 h	48 h	Lcat-1	15	1 h	48 h
Lca-10	10			Lcat-2		2 h	
Lca-15	15			Lcat-3		3 h	
Lca-20	20			Lcat-4		4 h	
Lca-25	25			Lcat-5		5 h	

20 Hz. The related parameters of the acoustic emission system were set as follows: threshold and pre-amplification values of 35 and 40 dB, respectively, pre-trigger value and impact definition time of 256 and 50 s, respectively, a sampling rate of 2 M, and an adjusted threshold voltage of 1 V. Two strain gauges were pasted on the coal surface and connected by a half-bridge, where Eg(+) and Eg(−) represented the positive and negative poles of the supplied bridge voltage, respectively, and Vi(+) represented the positive pole of the

signal.

3. Results and discussion

3.1. Crack morphology change in the coal cores

During the compression destruction process, the crack morphology of the coals showed the destroying patterns and degrees. The crack morphology mainly included the crack number, crack aperture, and crack distribution, etc., the more complex the crack distribution and the larger the crack number, the greater the deterioration degree of the coals. Fig. 4 showed the destruction features of the coals affected by the different impacts of liquid CO_2. By comparing coal LNA with an obvious crack, coal $LNCO_2$ was observed to have a large spallation area at the bottom end and some slippage at the fracture-side end. Fig. 4 (b) and (c) showed a similar failure pattern of 'axial separation' throughout the coal, and some dislocations along the fissure paths. Coal Lct-4 in Fig. 4 (d) showed an apparent spallation at the top end, with some fragments of various sizes also being visible, while coal Lct-5 was destroyed with separation along the side and some fragments at the bottom end. The coals shown in Fig. 4 (g)–(j) were broken with some damage profiles of 'separation + spallation', from which obvious vertical fissure zones and accompanying block sliding were observed. In detail, coal Lca-15 and Lca-25 showed multiple fissures parallel to the loading direction, with some block caving phenomenon appearing on the sides. In particular, coal Lca-25 was found to be damaged with many vertical splitting, while the coals shown in Fig. 4 (i) and (j) displayed some inclined cracks on the lateral surface, with some falling segments caused by the connection of cracks with different directions. Outburst zones were noticed to be generated in the coals of *ca* or *cat* series, where small sized segments were produced, indicating a severe degree of destruction.

The difference in the destruction profiles of the coals indicated that: a) the initial structure and anisotropy might create the diversity in coal destruction; b) the cold shock effect of cyclical liquid CO_2 increased the internal crack number, and the improvement in crack connection destroyed the coal structure, finally producing complex destruction forms [34,37,46]; and c) the temperature-adsorption coupling effect of liquid CO_2 jointly increased the internal crack volume of the coals and CO_2 adsorption quantity, which triggered more complex mechanical responses, because of the overall weakened structure and decrease in fissure friction [47].

3.2. Failure characteristics of different cores

During the compression failure process, the elasto-plastic deformation process included compaction, elastic, yield, and post-peak stages, which had unique σ-ε correlations at the corresponding stage [48,49]. Coal heterogeneity resulted in an uneven stress distribution, and a part of the released energy within the matrix was dissipated as heat and mechanical energy, while another part was released as elastic waves, known as acoustic emission phenomena, which has been commonly regarded as new crack generation and primary crack propagation [50,51]. There were some acoustic emission features, such as events, ring count, and energy, etc., where the event number represented the acoustic emission activity; ring count, as the number of ringing pulses exceeding the threshold value, reflected the frequency of acoustic emission events; and energy, as the cover area of the waveform, represented the intensity of the events [51]. The ring count and energy were selected in this study, along with the stress-strain (σ-ε) curves, to analyse the failure characteristics of the coals, as shown in Fig. 5.

Fig. 5 showed that diverse strain ratios and σ-ε curves of the coals occurred during the destruction process. In the compaction stage, some acoustic emission signals were observed because of the frictional compression among the primary micro-crack surfaces or uneven loads exerting on the crack spaces, indicating that some strain energy was released during the crack closure process [51]. As axial loads increased, some acoustic emission events were detected in the linear elastic stage, indicating the production of some micro-cracks, because of the generation of some local stress concentrations at the bottom loading end [50]. When the loads reached the yield strength, the rapid growth of acoustic emission characteristics implied that new cracks started to initiate and propagate with a quick strain energy release. At the stress peak point, drastic strength loss occurred and many acoustic emission events took

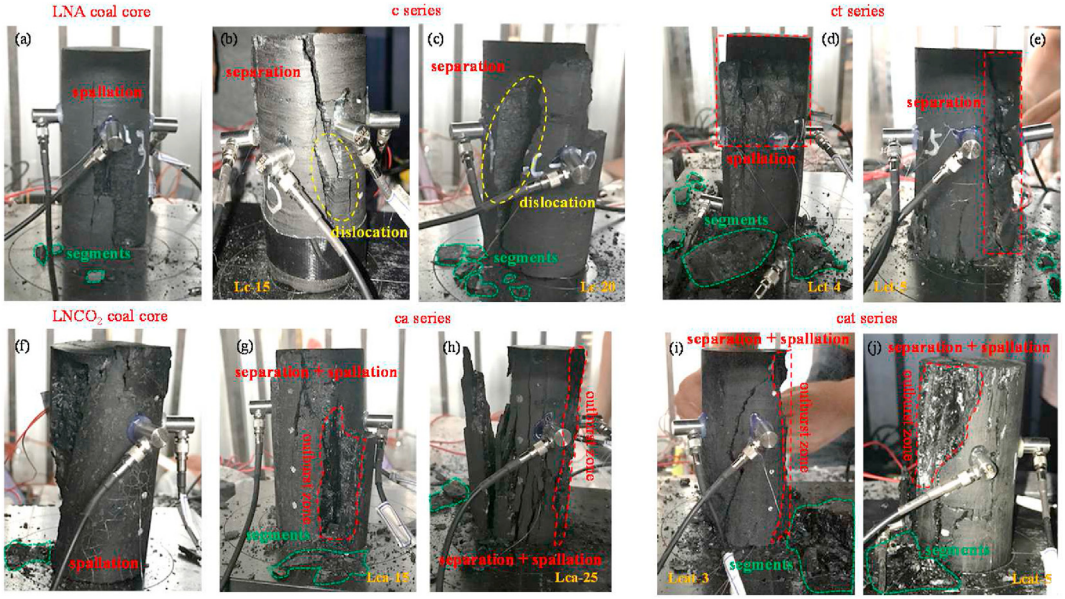

Fig. 4. Destruction features of coals under different conditions.

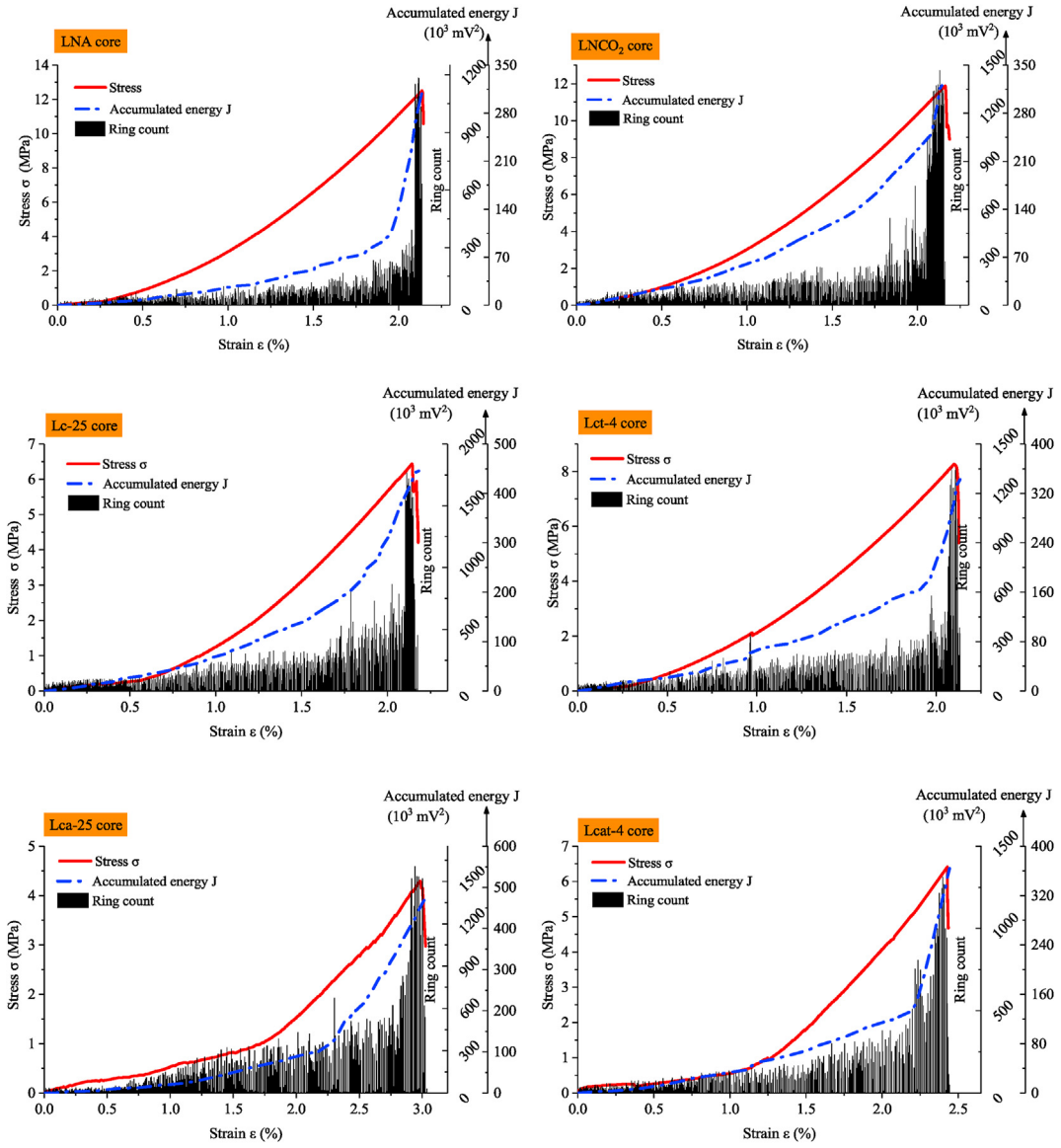

Fig. 5. Deterioration and acoustic emission features of the coals affected by liquid CO_2.

place, accompanied by a large amount of strain energy release, which indicated the increase in the crack propagation length [49].

The released energy could reflect the destruction degree of the coals, and comparing the energy amplitude difference between the raw and liquid CO_2 affected coals was necessary. By comparing the raw coal with the accumulated energy J of 309.2 $\times$ 10^3 mV^2, the CO_2 adsorbed coal showed a recorded J of 320.1 $\times$ 10^3 mV^2, while the J values of coal Lc-25 and Lct-4 were 445.36 $\times$ 10^3 and 342.17 $\times$ 10^3 mV^2, with the increase rates of 44.04% and 10.66%, respectively, and those of coal Lca-25 and Lcat-4 were 477.49 $\times$ 10^3 and 364.27 $\times$ 10^3 mV^2, with a growth rate of 54.43% and 17.81%, respectively. The increase in J indicated that liquid CO_2 could observably destroy the coal structure, with unrecoverable fatigue damage and cohesive stress deterioration caused by alternative temperature effects, and CO_2 adsorption occupied the formed crack networks, which further weakened the coal strength.

The differences between σ-ε curves and accompanying acoustic emission features indicated that the thermal cycling effect of liquid CO_2 could promote the original crack expansion and new crack generation, because of the conspicuous tensile stress between the grain joints. Based on temperature change $\triangle$T and thermal expansion coefficient α of the coals, the produced thermal strain $\varepsilon_{\text{thermal}}$ and thermal stress σ_{thermal} could be written as follows:

$$\begin{cases} \varepsilon_{thermal} = \alpha \Delta T \\ \sigma_{thermal} = E\varepsilon_{thermal} \end{cases} \tag{1}$$

A temperature gradient was easily produced between the cryogenic flow and coal matrix during the liquid CO_2 injection process, and thermal stress, at a distance of x_n from the borehole with different affecting time t_k, could be further inferred as:

$$\sigma(x_n, t_k) = \sum_{i=1,j=1}^{m} E\Delta\alpha_{ij}|t(x_n, t_k) - t(x_n, t_0)| \tag{2}$$

Based on the first and second laws of thermodynamics [52,53], the internal energy produced by CO_2 adsorption within the coal matrix was mainly transformed into thermal and strain energies. Myers [53] proposed that the energy change in the coal matrix followed the Gibbs and Helmholtz free energy equations, in fact,

the multiple sized pores within the matrix structure could be adsorbed by the number of CO_2 molecules. Perera and Ranjith [40] pointed out that CO_2 adsorption could decrease the coal strength, which could be explained by the Gibbs free energy theory and Griffith failure criteria, expressed as follows:

$$\begin{cases} d\gamma_s = -\eta d\xi \\ \sigma_t = \sqrt{\dfrac{2\gamma_s E}{\pi a}} \end{cases} \tag{3}$$

where η and $d\xi$ were the surface concentration and chemical potential change of the adsorbed CO_2, respectively; γ_s was the Gibbs free energy of the fracture length per unit, J/m^2; σ_t was the tensile stress required for new crack formation at the tip of the original pore, MPa; a was the half of the crack length, m; E was the elastic modulus, GPa.

The thermal cycling effect of liquid CO_2 caused uneven deformations in different grains and promoted larger damages to accumulate which further degraded the coal strength. Thermal fracture was considered to have two forms: new cracks generated nearly perpendicular to the native joint structure, and original crack propagation and connection to form complex crack networks. Based on this, the developed crack structure provided sufficient adsorption sites and spaces for CO_2 adsorption. The larger the CO_2 adsorption amount, the lower the Gibbs free energy of the matrix surface. The coupling effect of thermal cycling and adsorption of CO_2 significantly decreased the σ_t value, which could well evaluate the determination of crack initiation pressure and injectability of liquid CO_2 to achieve the goal of the scientific selection of injection parameters.

3.3. Mechanical responses of different coals

The σ-ε curve could qualitatively characterize the mechanical responses and destruction behaviours of the coals; for example, the ultimate strength of resistance to failure could be determined by compression stress σ_c, which was positively correlated with the coal matrix strength. The elastic modulus E could be calculated based on the fit correlation between σ and ε during the elastic stage, which might measure the ability to resist elastic deformation; the larger the E value, the greater the coal stiffness.

As shown in Fig. 6, the coals affected by liquid CO_2 with diverse parameters showed different mechanical responses, and the σ-ε curves of these coals showed 'concave type' trends with similar 'compaction stage - elastic stage - yield stage - post-peak stage' process. Compared to the σ_c and ε_c values (σ_c = 12.5 MPa and ε_c = 2.137%) of the raw coal, when the coals were affected by 5, 15, and 25 cycles, the Lc series coals had the corresponding values of 10.89 MPa and 2.052%, 9.48 MPa and 2.210%, and 5.94 MPa and 2.169%, respectively, while the Lca series coals had the σ_c and ε_c values of 11.09 MPa and 2.156%, 7.4 MPa and 2.544%, and 4.29 MPa and 2.984%, respectively. When the coals were influenced up to 2 and 4 h, the σ_c and ε_c values of Lct series coals were 10.87 MPa and 2.193%, 8.26 MPa and 2.099%, respectively, while those of Lcat series coals were 9.94 MPa and 2.278%, as well 6.41 MPa and 2.428%, respectively.

The decrease in σ_c and no obvious change in ε_c indicated individual variation in the diversity of the matrix structure and grain distribution, which affected the abilities to withstand loads and deformation failure. The alternating 'cold shock' and 'heating' steps made the temperature distribution uneven, and some tensile damages to occur in the grains because of the different thermal expansion coefficients, and further weakened the cohesive stress of matrix and decreased the σ_c value. Moreover, the crack number and complexity might have impacted coal destruction; for example, when most crack directions were approximately parallel to the axial direction, the coal might have mainly deformed by separation failure; when the crack direction was perpendicular to the axial direction, some slip might have occurred during the failure process. Increasing the crack volume and connection provided larger pore spaces for CO_2 adsorption and migration, thus, improving the CO_2 adsorption capacity. When large amounts of CO_2 were injected into the reservoir, CO_2 fluids first migrated along the pore-crack structure and were adsorbed on the pore surface, thus, finally promoting coal strength deterioration [47].

As shown in Fig. 7, the σ_c of coals LNA and LNCO$_2$ were 12.5 and 11.9 MPa, respectively, indicated that CO_2 adsorption could obviously decrease the coal strength because of gas slippage and lubrication. The σ_c values of liquid CO_2 affected coals were negatively correlated with increasing cyclical parameters, and σ_c scatters were fitted as a 'monotonic decreasing' trend, indicating that liquid CO_2 cyclical impacts could produce many micro-cracks, with the generation of new cracks and connection of new-raw cracks jointly destroying the coal structure. The decrease in the diversity of σ_c might be related to the original coal structure, stress response of the pore-cracks, and existing angle between the internal crack and loading directions might produce some stress concentration areas, facilitating the slippage to occur on the contact surface of the cracks. The greater the liquid CO_2 affecting extent, the more the damage accumulation, and the larger the decrease in the coal strength. The complete CO_2 adsorption within the crack networks decreased the friction and roughness of the cracks, and all deformations and damages increased during the loading process. When the ultimate deformation took place, the coal structure could be completely destroyed with larger strain energy release and crushing complexity.

3.4. Damage energy distribution of different cores

From the perspective of energy, the strain energy produced by continuous loads could be stored within the coal matrix. As shown in Fig. 8, the area bounded by the σ-ε curve could be regarded as the total energy J_t, which included the elastic energy J_e and dissipated energy J_r [54]. It was noticed that the area of the post-peak stage within the σ-ε curve was summarised as J_r because of the sharp drop in the curve of the coal material. The equations for calculating J_t, J_e, and J_r were as follows:

$$\begin{cases} J_t = J_e + J_r \\ J_t = \sum_{i=1}^{n} \dfrac{(\sigma_i + \Delta\sigma_i + \sigma_i)\Delta\varepsilon_i}{2} = \int_0^{\varepsilon_r} \sigma d\varepsilon J_e = \dfrac{\sigma_c^2}{2E} \end{cases} \tag{4}$$

Considering the anisotropy of individual coal, the rate of J_e/J_t and J_r/J_t were proposed to analyse energy evolution in terms of normalisation, which indirectly clarified the changes in coal structure and strength. Based on Equation (4), the J_e/J_t and J_r/J_t scatter distribution was shown in Fig. 9. With the impacts of cyclical liquid CO_2, different series coals had different energy proportions, and as the affecting cycles increased, the J_e/J_t and J_r/J_t scatters displayed a 'monotonical linear decrease' tendency and a 'monotonical linear increase' tendency, respectively. With the increasing affecting time, the J_e/J_t scatters of the Lct and Lcat series coals showed a 'dual linear-polynomial decrease' and a 'monotonical linear increase' trend, respectively, while the J_r/J_t scatters and affecting time had a similar decreasing fitting relationship.

The different relationship among the J_e/J_t, J_r/J_t scatters and cycle

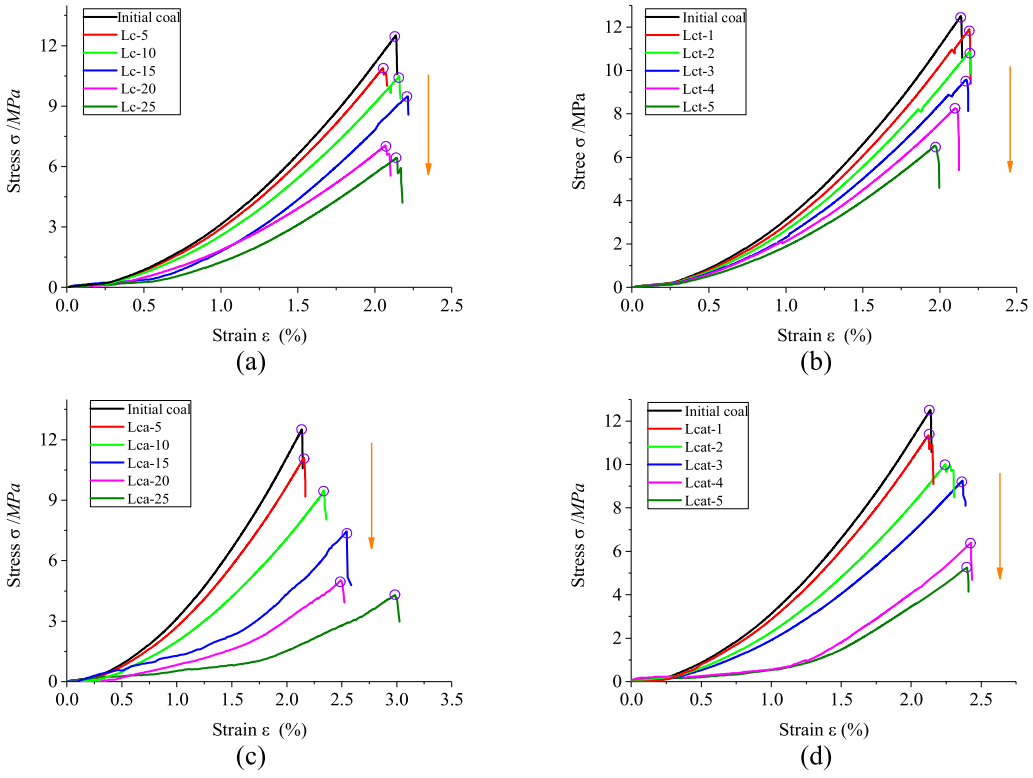

Fig. 6. σ-ε curves of coals affected by liquid CO_2 under different conditions.

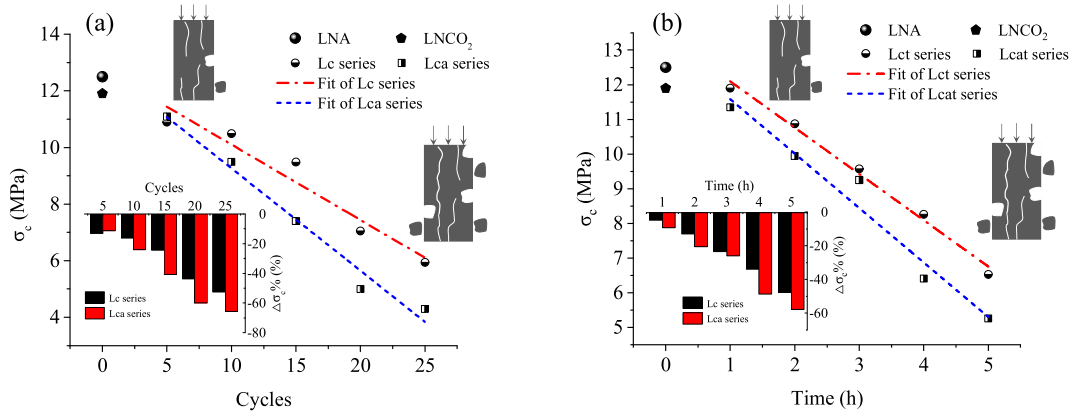

Fig. 7. Compressive stress σ_c and its change rate of coals with the increasing affecting parameters.

parameters indicated that the coal structures were destroyed under the coupling effect of thermal stress and adsorption of cyclical cryogenic CO_2 fluids. The alternating temperature shocks decomposed the binding forms among the grains because of tensile damage, and the adsorbed strain energy was allocated and transferred into elastic and dissipated energies based on the diverse strain responses. The uneven deformations of grain expansion/contraction made some strain components unrecoverable, with the residual strain gradually being accumulated after every cyclical affecting process. Meanwhile, the expansion/contraction of some phases might squeeze/stretch the other phases with different deformation capacities, and the expansion stress induced by CO_2 adsorption expansion behaviour of the coal matrix could fracture the non-expansion phase. Zhang et al. [55] verified this conclusion using the DEM models and predicted the tensile destruction behaviours of the mineral phase, and estimated that the maximum expansion stress in the filling area of the non-expanding phase could exceed 35 MPa, and concluded that the coupling effect of temperature-adsorption-stress loads could destroy the coal structure.

Fig. 10 showed the correlations between E, σ_c, elastic energy rate J_e/J_t, and dissipated energy rate J_r/J_t. When σ_c was constant, the J_e/J_t and J_r/J_t scatters positively and negatively correlated with E, respectively. Meanwhile, when E was constant, the J_e/J_t and J_r/J_t scatters showed positive and negative correlations with σ_c, respectively. It was noticed that the E range of 0.5—0.55 GPa and σ_c interval of [9.4 MPa, 9.5 MPa] showed an abnormal mutation, which might be greatly influenced by coal structure, parameters selected for the elastic stage, and negligible post-peak energy and strain. Due to larger porosity and greater anisotropy, the internal

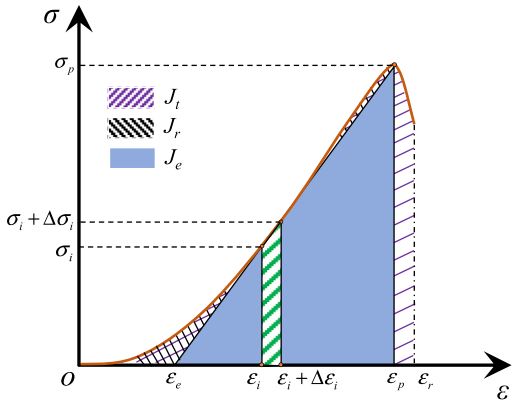

Fig. 8. Image of energy distribution based on σ-ε curve.

micro-cracks had smaller energy adsorption capacity, and most of the strain energy were dissipated as fracturing, slippage, and deformation [47,54].

The introduced energy analysis method indirectly reflected the impacts of cyclical liquid CO_2 on coal strength and structure, highlighting the storage and release capacity of strain energy for the affected cores. In field applications, monitoring the macro mechanical changes in the confined coal matrix under the effect of cyclical liquid CO_2 injection was necessary, and the energy analysis method could be used to evaluate the plastic region and damage extent through experimental tests conducted on σ-ε relations, while the strain energy evolution laws could help to systematically understand the correlations between coal structure transformation, injectability of liquid CO_2 and selection of cyclical parameters. Furthermore, the relationship between the rates of energy division and mechanical parameters might provide quantitative and fine characterisation of liquid CO_2 fracturing by analysing the accumulated strain energy and damage features.

3.5. Deterioration mechanism of the effects of cyclical liquid CO_2

Based on the above-mentioned analysis, a deterioration model (Fig. 11) of the effects of cyclical liquid CO_2 was established using the following hypothesis:

(1) The injected CO_2 fluids into the reservoirs were liquid with certain temperature-pressure condition;
(2) Micro-cracks existed at the radial directions of the borehole or horizontal well, and cryogenic CO_2 fluids with temperature T_f could migrate into the coal matrix with temperature T_m along the micro-crack directions;
(3) Crack structures were regarded as 'Hamburg Structure' without any water;
(4) Thermal fractures were conformed to tensile failure, and the capacities of heat conduction and expansion satisfied the first and second laws of thermodynamics;
(5) CO_2 adsorbed coals easily produce slippage under the compression process.

As shown in Fig. 11, the SEM images of the coal displayed some

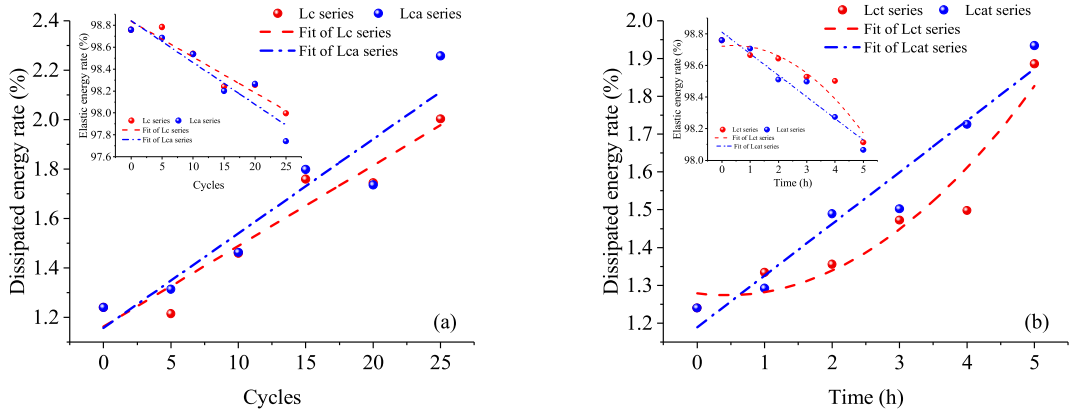

Fig. 9. Elastic energy rate J_e/J_t and dissipated energy rate J_r/J_t scatter distribution of the coals.

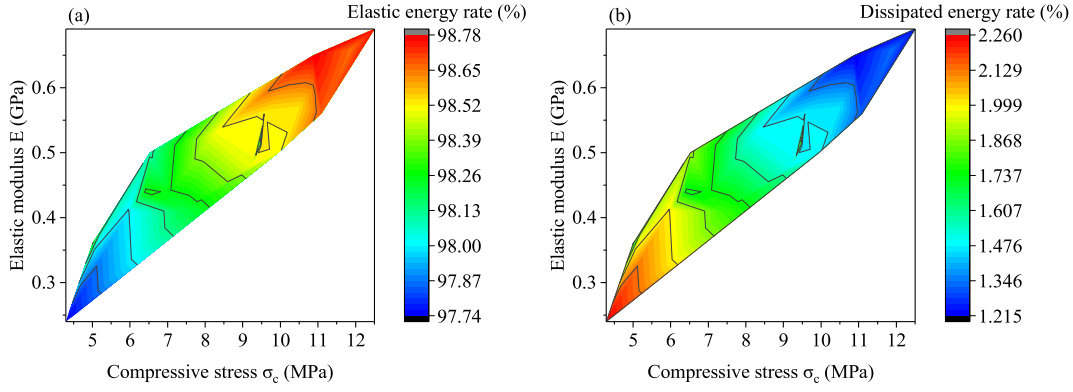

Fig. 10. Correlations between E, σ_c, elastic energy rate, and dissipated energy rate.

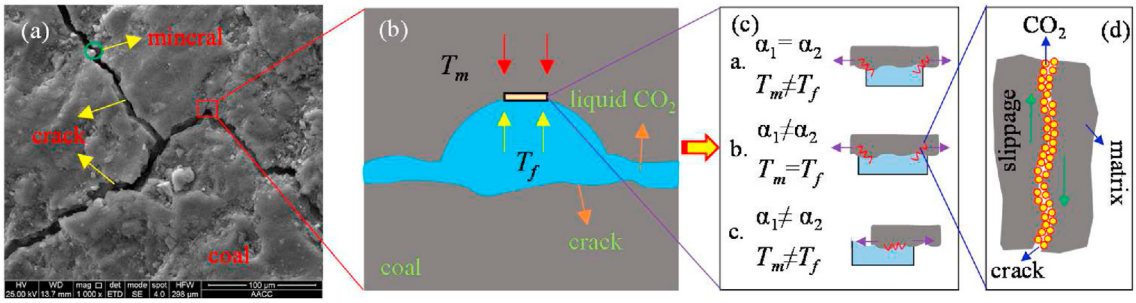

Fig. 11. Deterioration model of cyclical liquid CO_2 affecting.

micro-cracks and minerals, and micro-scale crack structure could be regarded as approximately parallel layers at the contact plane. When cryogenic liquid CO_2 flow fulfilled the cracks, the two layers with different features might have different deformations, based on the relationship among thermal stress, thermal expansion coefficients, and temperature difference (Equation (2)). When the coal-rock were loaded with constraints, the exerted heat-cold loads might exhibit low flexibility in the coal matrix, with the crustal stress being positively correlated with the ground temperature; the lower the temperature, the smaller the crustal stress [56]. The liquid CO_2 injection could actively reduce reservoir temperature, decreasing the in-situ stress and threshold value for crack development and propagation. Meanwhile, the increase in pore-pressure easily caused the primary compacted cracks to refracture under the coupling effect of thermal and crustal stresses, and the diversity in layer contraction obviously caused prominent tensile damage to accumulate and cohesive strength to deteriorate; subsequently, the more complex crack networks with larger region were formed, which in turn enlarged the low-temperature zone and increased the thermal fracturing events. In addition, the network of formed cracks provided abundant adsorption sites for CO_2 adsorption, and the increasing crack number decreased the damage resistance, high-pressure adsorption reduced the Gibbs free energy of the matrix surface, and coupled effect of tensile failure and shear slip finally significantly deteriorated the coal structure [40].

The produced network of cracks weakened the storage ability of the strain energy and increased the proportion of dissipated energy, such as kinetic and heat energies [57]. Under the effect of in-situ stress, the deteriorated coals might be destroyed with a large strain energy release, which increased the crack volume and permeability. Moreover, the energy distribution analysis accurately reflected the strain changes in the internal volume under the effect of cyclical liquid CO_2 injection, and the features of energy evolution deduced from the mechanical parameters were found to be significant in revealing the crack initiation mechanism, injection parameter selection and evaluation of liquid CO_2, thus, further improving the crack volume and enhancing the CBM recovery.

The potential mechanical damage of lignite was studied under the effects of cyclical liquid CO_2, and the obtained results reveal the mechanical response behaviours and facilitate the development of deterioration mechanism from the aspects of destruction patterns, change in related mechanical parameter, and evolution in the strain energy. However, some influencing factors, such as coal rank, water content, confining stress, and CO_2 phase, might have some effects on coal strength, and sufficient research needed to reveal the potential deterioration mechanism and determine the major influencing factors, optimal CO_2 injection parameter combination beneficial for the fracturing results, and quantitatively analyse the dynamic evolution of permeability.

4. Conclusions

(1) The coals affected by cyclical liquid CO_2 exhibited different destruction behaviours and fracture morphologies. The raw coal exhibited an obvious crack, and a large 'spallation' area with a certain slippage found in the CO_2 adsorption core. Coals affected by the impact of liquid CO_2 temperature showed a failure pattern of 'axial separation', while those influenced by the coupling effect of temperature -adsorption had a main 'separation and spallation' destruction form.

(2) Compared to the initial coal, the affected coals showed a larger ring count and accumulated energy, and σ_c decreased, indicating that thermal cycling and CO_2 adsorption could significantly promote crack generation and extension due to uneven temperature distribution, and the reduced Gibbs free energy increased the damage accumulation within the crack structure.

(3) The J_e/J_t scatters and J_r/J_t scatters positively and negatively correlated with the cyclical parameters and mechanical features (E and σ_c), respectively. This indicated that the greater the coal destruction, the smaller the strain energy storage capacity, and the larger the dissipated energy.

Credit author statement

Jizhao Xu: Conceptualization, Methodology, Writing – original draft preparation, Investigation. **Cheng Zhai**: Methodology, Writing – review & editing, Resources, Supervision. **Pathegama Gamage Ranjith**: Writing – review & editing. **Shuxun Sang**: Methodology, Writing – review & editing. **Yong Sun**: Validation, Investigation. **Yuzhou Cong**: Data curation, Visualization. Wei Tang: Data curation, Visualization. **Yangfeng Zheng**: Investigation, Data curation.

Declaration of competing interest

The authors declare that they have no known competing financial interests or personal relationships that could have appeared to influence the work reported in this paper.

Acknowledgement

This paper is financially supported by the Open Fund of Jiangsu Key Laboratory of Coal-based Greenhouse Gas Control and Utilization (2019A002, 2020KF06), China Postdoctoral Science Foundation (2021M693409), the National Natural Science Foundation of China (52104228, 51774278), and the National Science Fund for Distinguished Young Scholars (51925404).

References

[1] Moore TA. Coalbed methane: a review. Int J Coal Geol 2012;101:36–81.
[2] Rathi R, Priya A, Vohra M, et al. Development of a microbial process for methane generation from bituminous coal at thermophilic conditions. Int J Coal Geol 2015;147–148:25–34.
[3] Zou QL, Liu H, Cheng ZH, et al. Effect of slot inclination angle and borehole-slot ratio on mechanical property of pre-cracked coal: implications for ECBM recovery using hydraulic slotting. Nat Resour Res 2020;29:1705–29.
[4] Wen H, Wang H, Fan SX, et al. Improving coal seam permeability and displacing methane by injecting liquid CO_2: an experimental study. Fuel 2020;281:118747.
[5] Qin L, Li SG, Zhai C, et al. Changes in the pore structure of lignite after repeated cycles of liquid nitrogen freezing as determined by nitrogen adsorption and mercury intrusion. Fuel 2020;267:117214.
[6] Hu QT, Liu L, Li QG, et al. Experimental investigation on crack competitive extension during hydraulic fracturing in coal measures strata. Fuel 2020;265:117003.
[7] Xu JZ, Zhai C, Qin L. Pulse hydraulic fracturing technology and its application in coalbed methane extraction. Int J Oil Gas Coal Technol 2018;19:115–33.
[8] Xie JN, Xie J, Ni GH, et al. Effects of pulse wave on the variation of coal pore structure in pulsating hydraulic fracturing process of coal seam. Fuel 2020;264:116906.
[9] Lin BQ, Zou QL, Liang YP, et al. Response characteristics of coal subjected to coupling static and waterjet impact loads. Int J Rock Mech Min Sci 2018;103:155–67.
[10] Cha MS, Yin XL, Kneafsey T, et al. Cryogenic fracturing for reservoir stimulation – Laboratory studies. J Petrol Sci Eng 2014;124:436–50.
[11] Ranathunga AS, Perera MSA, Ranjith PG, et al. A macro-scale experimental study of sub- and super-critical CO_2 flow behaviour in Victorian brown coal. 20115, 158: 864-873.
[12] Cao YX, Zhang JS, Zhai H, et al. CO_2 gas fracturing: a novel reservoir stimulation technology in low permeability gassy coal seams. Fuel 2017;203:197–207.
[13] Yang XL, Wen GC, Lu TK, et al. Optimization and field application of CO_2 gas fracturing technique for enhancing CBM extraction. Nat Resour Res 2020;29:1875–96.
[14] Xu JZ, Zhai C, Qin L, et al. Evaluation research of the fracturing capacity of non-explosive expansion material applied to coal-seam roof rock. Int J Rock Mech Min Sci 2017;94:103–11.
[15] Li H, Shi SL, Lin BQ, et al. Effects of microwave-assisted pyrolysis on the microstructure of bituminous coals. Energy 2019;187:115986.
[16] Li H, Shi SL, Lin BQ, et al. A fully coupled electromagnetic, heat transfer and multiphase porous media model for microwave heating of coal. Fuel Process Technol 2019;189:49–61.
[17] Perera M, Samintha A. Influences of CO_2 injection into deep coal seams: a review. Energy Fuel 2017;31:10324–34.
[18] Xu JZ, Zhai C, Liu SM, et al. Feasibility investigation of cryogenic effect from liquid carbon dioxide multi cycle fracturing technology in coalbed methane recovery. Fuel 2017;206:371–80.
[19] Vilarrasa V, Silva O, Carrera J, et al. Liquid CO_2 injection for geological storage in deep saline aquifers. Int J Greenh Gas Control 2013;14:84–96.
[20] Silva O, Carrera J, Vilarrasa V. An efficient injection concept for the geological storage of CO_2. In: 6th trondheim CCS conference; 2011. Trondheim, Norway, 14-16 June.
[21] Vilarrasa V, Jonny Rutqvist. Thermal effects on geologic carbon storage. Earth Sci Rev 2017;165:245–56.
[22] Feng GH. Process analyses and numerical models for multiphase flow and phase change in CO2-ECBM engineering. Doctoral dissertation. Jilin University; 2018.
[23] Krogh E, Nilsen R, Henningsen R. Liquefied CO_2 injection model. Energy Procedia 2012;23:527–55.
[24] Ma L, Wei GM, Wang S, et al. Experimental study of displacing & replacing methane in low permeability coal seam by injecting liquid carbon dioxide. J Chongqing Univ 2018;41:76–83.
[25] Roy P, Walsh DCS, Morris JP, et al. Studying the impact of thermal cycling on wellbore integrity during CO_2 injection. In: the 50th US rock mechanics/geomechanics symposium; 2016. Houston, Texas, USA, 26-29 June.
[26] Teodoriu. Why and when does casing fail in geothermal wells: a surprising question?. In: Proceedings of world geothermal congress 2015; 2015. Melboune, Australia, 19-25 April.
[27] Kaldal GS, Jónsson Mþ, Pálsson H, et al. Structural analysis of casings in high temperature geothermal wells in Iceland. In: Proceedings of world geothermal congress 2015; 2015. Melboune, Australia, 19-25 April.
[28] Li ZB. Thermal cracking and displacement for enhancing methane extraction by phase transition of liquid CO_2 injection in coal seam. Doctoral dissertation. Xi'an University of Science and Technology; 2017.
[29] Park C, Synn JH, Shin HS, et al. An experimental study on the thermal characteristics of rock at low temperatures. Int J Rock Mech Min Sci 2004;41:367–8.
[30] Zhang HM, Meng XZ, Peng C, et al. Rock damage constitutive model based on residual intensity characteristics under freeze-thaw and load. J China Coal Soc 2019;44:3404–11.
[31] Yang ZZ, Zhang YP, Jia M, et al. Experimental Research on influence of low temperature on coal permeability. Rock Soil Mech 2017;38:354–60.
[32] Qin L, Zhai C, Liu SM, et al. Failure mechanism of coal after cryogenic freezing with cyclic liquid nitrogen and its influences on coalbed methane exploitation. Energy Fuel 2016;30(10):8567–78.
[33] Xu JZ, Zhai C, Liu SM, et al. Pore variation of three different metamorphic coals by multiple freezing-thawing cycles of liquid CO_2 injection for coalbed methane recovery. Fuel 2017;208:41–51.
[34] Xu JZ, Zhai C, Liu SM, et al. Investigation of temperature effects from LCO_2 with different cycle parameters on the coal pore variation based on infrared thermal imagery and low-field nuclear magnetic resonance. Fuel 2018;215:528–40.
[35] Xu JZ, Zhai C, Qin L, et al. Characteristics of pores under the influence of cyclic cryogenic liquid carbon dioxide using low-field nuclear magnetic resonance. Geofluids 2018;2018:1–14.
[36] Wen H, Li ZB, Deng J, et al. Influence on coal pore structure during liquid CO_2-ECBM process for CO_2 utilization. J CO2 Util 2017;21:543–52.
[37] Wen H, Wei GM, Ma L, et al. Damage characteristics of coal microstructure with liquid CO_2 freezing-thawing. Fuel 2019;249:169–77.
[38] Viete DR, Ranjith PG. The effect of CO_2 on the geomechanical and permeability behaviour of brown coal: implications for coal seam CO_2 sequestration. Int J Coal Geol 2006;66:204–16.
[39] Viete DR, Ranjith PG. The mechanical behaviour of coal with respect to CO_2 sequestration in deep coal seams. Fuel 2007;86(17–18):2667–71.
[40] Perera MSA, Ranjith PG. Carbon dioxide sequestration effects on coal's hydro-mechanical properties: a review. Int J Energy Res 2012;36:1015–31.
[41] Larsen JW. The effects of dissolved CO_2 on coal structure and properties. Int J Coal Geol 2004;57(1):63–70.
[42] Bai B, Li XC, Liu YF, et al. Preliminary theoretical study on impact on coal caused by interactions between CO_2 and coal. Rock Soil Mech 2007;28:823–6.
[43] Liu YB, Yin GZ, Li MH, et al. Mechanical properties and failure behavior of dry and water-saturated anisotropic coal under true-triaxial loading conditions. Rock Mech Rock Eng 2020;53:4799–818.
[44] Qin L, Zhai C, Liu SM, et al. Factors controlling the mechanical properties degradation and permeability of coal subjected to liquid nitrogen freeze-thaw. Sci Rep 2017;7:3675.
[45] Ministry of Land and Resources PRC. Test rules for physical and mechanical properties of rocks. Part 18: uniaxial compressive strength test of rocks. 2015.
[46] Xu JZ, Zhai C, Ranjith PG, et al. Petrological and ultrasonic velocity changes of coals caused by thermal cycling of liquid carbon dioxide in coalbed methane recovery. Fuel 2019;249:15–26.
[47] Zhu WC, Liu LY, Liu JS, et al. Impact of gas adsorption-induced coal damage on the evolution of coal permeability. Int J Rock Mech Min Sci 2018;101:89–97.
[48] Bruning T, Karakus M, Nguyen GD, et al. An experimental and theoretical stress-strain-damage correlation procedure for constitutive modelling of granite. Int J Rock Mech Min Sci 2019;116:1–12.
[49] Manso J, Marcelino J, Caldeira L. Effect of the clump size for bonded particle model on the uniaxial and tensile strength ratio of rock. Int J Rock Mech Min Sci 2019;114:131–40.
[50] Wang ZH, Wang JC, Yang SL, et al. Failure behaviour and acoustic emission characteristics of different rocks under uniaxial compression. J Geophys Eng 2020;17:76–88.
[51] Jia ZQ, Xie HP, Zhang R, et al. Acoustic emission characteristics and damage evolution of coal at different depths under triaxial compression. Rock Mech Rock Eng 2020;53:2063–76.
[52] Tuin G, Stein HN. The excess Gibbs free energy of adsorption of sodium dodecylbenzenesulfonate on polystyrene particles. Langmuir 1995;11:1284–90.
[53] Myers AL. Thermodynamics of adsorption in porous materials. AIChE J 2002;48:145–60.
[54] Sampath KHSM, Perera MSA, Li DY, et al. Evaluation of the mechanical behaviour of brine + CO_2 saturated brown coal under mono-cyclic uni-axial compression. Eng Geol 2019;263:105312.
[55] Zhang Yihuai, Zhang Zike, Mohammad Sarmadivaleh, et al. Micro-scale fracturing mechanisms in coal induced by adsorption of supercritical CO_2. Int J Coal Geol 2017;175:40–50.
[56] Enayatpour S, Oort VE, Patzek T. Thermal cooling to improve hydraulic fracturing efficiency and hydrocarbon production in shales. J Nat Gas Sci Eng 2019;62:184–201.
[57] Li ZB, Wang FS, Shu CM, et al. Damage effects on coal mechanical properties and micro-scale structures during liquid CO_2-ECBM process. J Nat Gas Sci Eng 2020;83:103579.